

Article

Comparative Thermal Degradation Behaviors and Kinetic Mechanisms of Typical Hardwood and Softwood in Oxygenous Atmosphere

Xiaokang Xu, Renming Pan and Ruiyu Chen * 

School of Chemistry and Chemical Engineering, Nanjing University of Science and Technology, Nanjing 210094, China; xiaokangxu@njust.edu.cn (X.X.); 12016042@njust.edu.cn (R.P.)

* Correspondence: crynjjust@njust.edu.cn; Tel.: +86-025-8430-3159

Abstract: In order to utilize woody biomass effectively for bioenergy and chemical feedstocks, the comparative thermal degradation behaviors and kinetic mechanisms of typical hardwood (beech wood) and softwood (camphorwood) were studied at various heating rates in air. The Kissinger-Akahira-Sunose approach combined with the Coats-Redfern approach was employed to estimate the kinetic triplet. Softwood degradation began and ended at lower temperatures than hardwood. Compared with softwood, the maximal reaction rate of hardwood was greater and occurred in the higher temperature region. Two decomposition regions were determined by the variation of activation energy, and the dividing point was $\alpha = 0.6$ and $\alpha = 0.65$ for hardwood and softwood, respectively. Moreover, the average activation energy of hardwood was larger than that of softwood during the whole decomposition process. The thermal degradation process occurring in region 1 was dominated by the Avrami-Erofeev and 3D diffusion models for hardwood and softwood, respectively. Furthermore, the kinetic modeling results showed good consistency between the experimental and simulated curves under 5, 15, 20, and 40 K/min. It is noted that the thermogravimetric experimental profile under 20 K/min was not used for estimating the kinetic triplet. Besides, the combustion performance of hardwood is superior to softwood under the same external conditions (heating rate and atmosphere).

Keywords: thermal degradation; woody biomass; bioenergy; renewable energy; thermogravimetric analysis



Citation: Xu, X.; Pan, R.; Chen, R. Comparative Thermal Degradation Behaviors and Kinetic Mechanisms of Typical Hardwood and Softwood in Oxygenous Atmosphere. *Processes* **2021**, *9*, 1598. <https://doi.org/10.3390/pr9091598>

Academic Editor: Jorge Cunha

Received: 18 August 2021

Accepted: 2 September 2021

Published: 6 September 2021

Publisher's Note: MDPI stays neutral with regard to jurisdictional claims in published maps and institutional affiliations.



Copyright: © 2021 by the authors. Licensee MDPI, Basel, Switzerland. This article is an open access article distributed under the terms and conditions of the Creative Commons Attribution (CC BY) license (<https://creativecommons.org/licenses/by/4.0/>).

1. Introduction

In recent decades, the rapid development of industry is driven by the consumption of a large number of energy resources, mainly fossil energy. The large consumption of fossil energy will lead to energy shortages or even energy crisis, and cause serious air pollution and climate change [1–3]. Since the industrial revolution, the concentration of carbon dioxide in the atmosphere has increased by nearly 30% [4], which is widely considered to be the main cause of the greenhouse effect [5]. The biomass utilization for bioenergy can help to reduce the emission of greenhouse gases and other toxic and harmful gases [6,7], and reduce the dependence of social development on fossil energy [8,9]. As a representative renewable biomass, woody biomass is anticipated to take on an increasingly significant role in the production of bioenergy (such as biochar and biogas) and chemical feedstocks [10,11].

Combustion, as a simple and effective thermochemical conversion technology for solid materials' utilization [12–14], is widely used in heat and electric energy production [15,16]. The combustion of solid materials involves a series of complex redox reactions, and it is mainly affected by the external factors [17–19] (such as heating rate and temperature) and internal factors [20,21] (compositions of solid materials). It has been widely reported that woody biomass is mainly composed of hemicellulose, cellulose, and lignin [22–24]. The structure characteristics and physicochemical properties of these three compositions have

a great effect on the thermal degradation behaviors of wood [25,26]. Woody biomass can be divided into two broad categories, containing hardwood and softwood [12], and the contents of the three main components (hemicellulose, cellulose, and lignin) in these two categories are quite different.

In order to reveal the differences in thermal decomposition characteristics and kinetics between hardwood and softwood, many studies have been carried out. Ding et al. [27] focused on the thermal decomposition characteristics and kinetic mechanisms of hardwood and softwood by thermogravimetric analysis in nitrogen. The obtained activation energy of softwood was greater than that of hardwood during the whole pyrolysis process, and the kinetic mechanisms for both hardwood and softwood can be summed up as a diffusion mechanism followed by a reaction order mechanism. Yao et al. [28] calculated the apparent activation energy of hardwood and softwood in nitrogen atmosphere, and the mean values were approximately 155 and 160 kJ/mol for hardwood and softwood, respectively. Zadeh et al. [29] conducted the pyrolysis experiments and characterized the products generated from hardwood and softwood lignin in nitrogen. The results showed that the bio-oil and biochar yields of softwood lignin were higher than hardwood lignin, while the gas yield of softwood lignin was lower than hardwood lignin. Moreover, Asmadi et al. [30] identified the pyrolysis behaviors of hardwood and softwood in nitrogen and showed that hardwood formed more volatiles (tar) instead of char in the primary pyrolysis stage, and the tar-to-gas conversion rates for hardwoods in the secondary reaction stage were smaller than those of softwood. Gronli et al. [31] studied the thermal decomposition characteristics of 4 types of hardwood and 5 types of softwood in nitrogen and indicated that the hardwood degradation initiated at higher temperatures and the degradation regions of hemicellulose and cellulose were narrower compared with those of softwood.

According to the above-mentioned literature, the differences of thermal decomposition behaviors and kinetics between hardwood and softwood in inert atmosphere do exist and have been revealed. It should be noted that the thermal degradation characteristics, activation energy, and kinetic mechanisms of woody biomass under oxidative atmosphere are quite diverse from those under inert atmosphere. In fact, the thermal degradation of solid materials in oxidizing atmosphere is more complicated because the presence of oxidants (air, oxygen, etc.) will produce heterogeneous reactions between oxygen and solid reactants and homogeneous reactions between oxygen and volatiles [27,32–34]. However, to our best knowledge, there are significantly few studies focusing on the differences of the thermal degradation characteristics, kinetic parameters, and kinetic mechanisms between hardwood and softwood under air atmosphere to date.

In our work, the thermal degradation behaviors and kinetic mechanisms of typical hardwood (beech wood) and softwood (camphorwood) were investigated by employing a thermogravimetric analyzer at multiple heating rates in air. The Kissinger-Akahira-Sunose [35,36] approach was employed to attain the apparent activation energy and the Coats-Redfern [37] approach was used for estimating the kinetic mechanisms. In addition, the kinetic modeling for hardwood and softwood decomposition was also conducted in this work.

2. Materials and Methods

2.1. Materials

Beech wood has beautiful color and texture, as well as high hardness, which is often used in furniture, wooden doors, floors, and handicrafts. In addition, beech wood also has the advantages of good load-bearing performance and good compression resistance, which is often used in shipbuilding, construction, and bridges. Beech wood (*Fagus sylvatica*) is selected as the representative hardwood in the present study. Camphorwood, as used before [38], is considered as the typical softwood, which is used in the present work. Beech wood and camphorwood were sampled from Europe and China, respectively. All the wood samples used in the experiment are the center layers of wood. Before the thermogravimetric experiment, the beech wood and camphorwood were first pulverized into sawdust with

a mill, and then sawdust with particle size in the range of 0.154–0.2 mm was screened out with 75- and 100-mesh screens as the experimental samples. Finally, the sawdust was placed in the oven and dried at 378.15 K for 24 h to completely remove the free water.

2.2. Thermogravimetric Experiments

The comparison of the thermal degradation behaviors between beech wood and camphorwood was conducted by a thermogravimetric analyzer (SDTA 851E) at 5, 15, 20, and 40 K/min under air atmosphere. In each test, the specimen mass was approximately 5 mg, and was heated from 300 to 1000 K. Air was used for the tests at a flow rate of 60 mL/min.

2.3. Kinetic and Thermodynamic Analyses

The integral approaches were adopted for estimating the kinetic triplet during the thermal decomposition process of beech wood and camphorwood. The kinetic equations can be expressed as follows:

$$\frac{d\alpha}{dt} = k(T)f(\alpha) \quad (1)$$

where α is the conversion degree, t is the reaction time and T is the reaction temperature, $k(T)$ is the reaction rate constant, and $f(\alpha)$ is the function of the kinetic mechanism. α and $k(T)$ can be thus obtained as:

$$\alpha = (m_0 - m_t)/(m_t - m_\infty) \quad (2)$$

where m_0 , m_t , and m_∞ are the initial, actual, and final masses of the specimens, respectively.

Based upon the Arrhenius equation, $k(T)$ can be described as the following expression:

$$k(T) = A \exp\left(-\frac{E_\alpha}{RT}\right) \quad (3)$$

where A and E_α are the pre-exponential factor and activation energy respectively, and R is the universal gas constant (8.314 J/(mol·K)).

A constant heating rate ($\beta = dT/dt$) was performed in a non-isothermal reaction process. Thus, Equation (1) can be rewritten as follows according to Equation (3):

$$\frac{d\alpha}{dT} = \frac{A}{\beta} \exp\left(-\frac{E_\alpha}{RT}\right) f(\alpha) \quad (4)$$

The following equation can be obtained by integrating the two ends of Equation (4):

$$g(\alpha) = \int_0^\alpha \frac{d\alpha}{f(\alpha)} = \frac{A}{\beta} \int_0^{T_\alpha} \exp\left(-\frac{E_\alpha}{RT}\right) dT = \frac{AE_\alpha}{\beta R} \int_{y_\alpha}^\infty \frac{\exp(-y)}{y^2} dy = \frac{AE_\alpha}{\beta R} p(y) \quad (5)$$

where $g(\alpha)$ is the function of the kinetic mechanism in its integral form.

Model-free methods (such as Kissinger-Akahira-Sunose [35,36]) can obtain the accurate activation energy, but cannot attain the pre-exponential factor and kinetic mechanism. Model-matching methods (such as Coats-Redfern [37]) are usually adopted to calculate the pre-exponential factor and activation energy with one certain kinetic model [39]. In this work, the KAS method coupled with the CR method was used for estimating the kinetic triplet.

2.3.1. Kissinger-Akahira-Sunose Approach

The KAS approach [35,36] is one integral approach and can be expressed as below:

$$\ln\left(\frac{\beta}{T_\alpha^2}\right) = \ln\left(\frac{A_\alpha R}{E_\alpha g(\alpha)}\right) - \frac{E_\alpha}{RT_\alpha} \quad (6)$$

The same α is chosen at different heating rates, so that the linear relationship occurs between $\ln(\beta/T_\alpha^2)$ and $1/T$, then E_α values are acquired from its slope of $-E_\alpha/R$.

2.3.2. Coats-Redfern Approach

The CR approach [37] is one popular model-fitting approach for estimating the kinetic mechanisms and parameters (E and A). Based upon an asymptotic approximation $RT/E_\alpha \rightarrow 0$, this approach can be expressed as follows:

$$\ln\left(\frac{g(\alpha)}{T_\alpha^2}\right) = \ln\left(\frac{A_\alpha R}{\beta E_\alpha}\right) - \frac{E_\alpha}{RT_\alpha} \quad (7)$$

E and A can be obtained from the slope and intercept of the plots ($\ln(g(\alpha)/T_\alpha^2)$ versus $1/T$). Table 1 lists the various functions of kinetic mechanisms for the thermal decomposition of solid materials [40–43].

Table 1. Kinetic models/mechanisms.

No.	$g(\alpha)$	$f(\alpha)$	Kinetic Mechanism
1. Power law			
1	$\alpha^{3/2}$	$2/3\alpha^{-1/2}$	Nucleation
2	$\alpha^{1/2}$	$2\alpha^{1/2}$	Nucleation
3	$\alpha^{1/3}$	$3\alpha^{2/3}$	Nucleation
4	$\alpha^{1/4}$	$4\alpha^{3/4}$	Nucleation
2. Reaction order			
5	$-\ln(1-\alpha)$	$1-\alpha$	Assumed random nucleation and its subsequent growth
6	$(1-\alpha)^{-1}-1$	$(1-\alpha)^2$	Chemical reaction
7	$(1-\alpha)^{-2}-1$	$1/2(1-\alpha)^3$	Chemical reaction
3. Avrami-Erofeev			
8	$[-\ln(1-\alpha)]^{2/3}$	$3/2(1-\alpha)[- \ln(1-\alpha)]^{1/3}$	Assumed random nucleation and its subsequent growth
9	$[-\ln(1-\alpha)]^{1/2}$	$2(1-\alpha)[- \ln(1-\alpha)]^{1/2}$	Assumed random nucleation and its subsequent growth
10	$[-\ln(1-\alpha)]^{1/3}$	$3(1-\alpha)[- \ln(1-\alpha)]^{2/3}$	Assumed random nucleation and its subsequent growth
11	$[-\ln(1-\alpha)]^{1/4}$	$4(1-\alpha)[- \ln(1-\alpha)]^{3/4}$	Assumed random nucleation and its subsequent growth
12	$[-\ln(1-\alpha)]^2$	$1/2(1-\alpha)[- \ln(1-\alpha)]^{-1}$	Assumed random nucleation and its subsequent growth
13	$[-\ln(1-\alpha)]^3$	$1/3(1-\alpha)[- \ln(1-\alpha)]^{-2}$	Assumed random nucleation and its subsequent growth
14	$[-\ln(1-\alpha)]^4$	$1/4(1-\alpha)[- \ln(1-\alpha)]^{-3}$	Assumed random nucleation and its subsequent growth
4. Contracting			
15	$1-(1-\alpha)^{1/2}$	$2(1-\alpha)^{1/2}$	Contracting cylinder (cylindrical symmetry)
16	$1-(1-\alpha)^{1/3}$	$3(1-\alpha)^{2/3}$	Contracting sphere (spherical symmetry)
5. Diffusion			
17	α^2	$1/2\alpha$	One-dimensional diffusion
18	$\alpha + (1-\alpha)\ln(1-\alpha)$	$[-\ln(1-\alpha)]^{-1}$	Two-dimensional diffusion
19	$1-2/3\alpha-(1-\alpha)^{2/3}$	$(3/2)[(1-\alpha)^{-1/3}-1]^{-1}$	Three-dimensional diffusion, cylindrical symmetry
20	$[(1-\alpha)^{-1/3}-1]^2$	$(3/2)(1-\alpha)^{4/3}[(1-\alpha)^{-1/3}-1]^{-1}$	Three-dimensional diffusion

E_α and A estimates gained by the above two kinetic approaches are employed to compute the changes in enthalpy (ΔH), Gibbs free energy (ΔG), and entropy (ΔS), expressed as [44]:

$$\Delta H = E_\alpha - RT_\alpha \quad (8)$$

$$\Delta G = E_\alpha + RT_p \ln\left(\frac{K_B T_p}{hA}\right) \quad (9)$$

$$\Delta S = \frac{\Delta H - \Delta G}{T_p} \quad (10)$$

where K_B is the Boltzmann constant (1.381×10^{-23} J/K), h is the Plank constant (6.626×10^{-34} J·s), and T_p is peak temperature.

2.4. Determination of Combustion Characteristic Parameters

Thermogravimetric experiments can record the mass loss of biomass during the heating process in real time, which is used to draw the TG (mass loss) and DTG (mass loss rate) curves. From these curves, the thermal parameters of the biomass combustion process can be obtained directly, including ignition temperature (T_i), peak temperature (T_{max}), and burnout temperature (T_b). These parameters reveal the thermal behavior of biomass during the combustion process, and describe the beginning and end of combustion.

As shown in Figure 1, the ignition temperature (T_i) is defined as follows: Firstly, a vertical line is drawn through the DTG peak point and intersects with the TG curve at point O. Then, the tangent line of the TG curve at point O is made and intersects with the extension line of the initial horizontal line of the TG curve at point M. Finally, a vertical line is made through point M to intersect with abscissa at point N, and the corresponding temperature of point N is the ignition temperature, T_i .

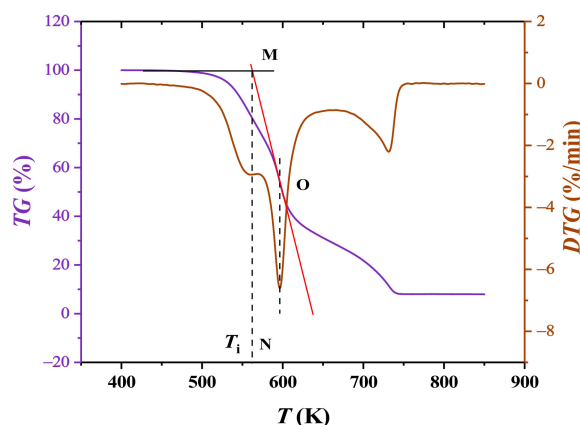


Figure 1. The illustration of ignition temperature (T_i).

The peak temperature (T_{max}) is the temperature at the peak of the DTG curve, while the burnout temperature (T_b) corresponds to the temperature at the end of the DTG curve (1% mass loss rate).

3. Results and Discussions

3.1. Thermogravimetric Analyses

Figure 2a,b illustrates the reaction rate ($d\alpha/dT$) curves of hardwood (beech wood) and softwood (camphorwood) specimens at 5, 15, and 40 K/min, respectively. Softwood began to decompose earlier than hardwood, and the thermal degradation process of softwood ended earlier than that of hardwood. There is one shoulder and two distinct peaks on the $d\alpha/dT$ curves. The hardwood shoulder occurred at a lower temperature than that of softwood, but the two peaks of hardwood appeared at a higher temperature than that of softwood. Moreover, the shoulder values of hardwood were smaller than those of softwood, but the first peak values of hardwood were larger than those of softwood. In addition, the heating rates had an important influence on the locations and values of the peaks, but it did not change the patterns of the reaction rate curves. The peaks and shoulder moved towards the high-temperature regions for both hardwood and softwood with the elevated heating rate. The reaction rate value of the shoulder rarely varied with the heating rate, and the first peak value declined with the heating rate while the second peak value first increased and then decreased with the heating rate. It is noted that there is an obvious “shoulder” region for softwood at a lower heating rate compared with that at a higher heating rate. Figure 2c,d presents the curves of conversion degree, α , under

multiple heating rates for beech and camphorwood, respectively. Moreover, the detailed information about the decomposition characteristics for hardwood and softwood are listed in Table 2. At the same heating rate, the shoulder of hardwood appeared earlier than that of softwood, while the two peaks appeared later. To further show the differences between the two types of wood, the $d\alpha/dT$ curves of beech and camphorwood under 5 and 40 K/min are comparatively presented in Figure 3a,b, respectively.

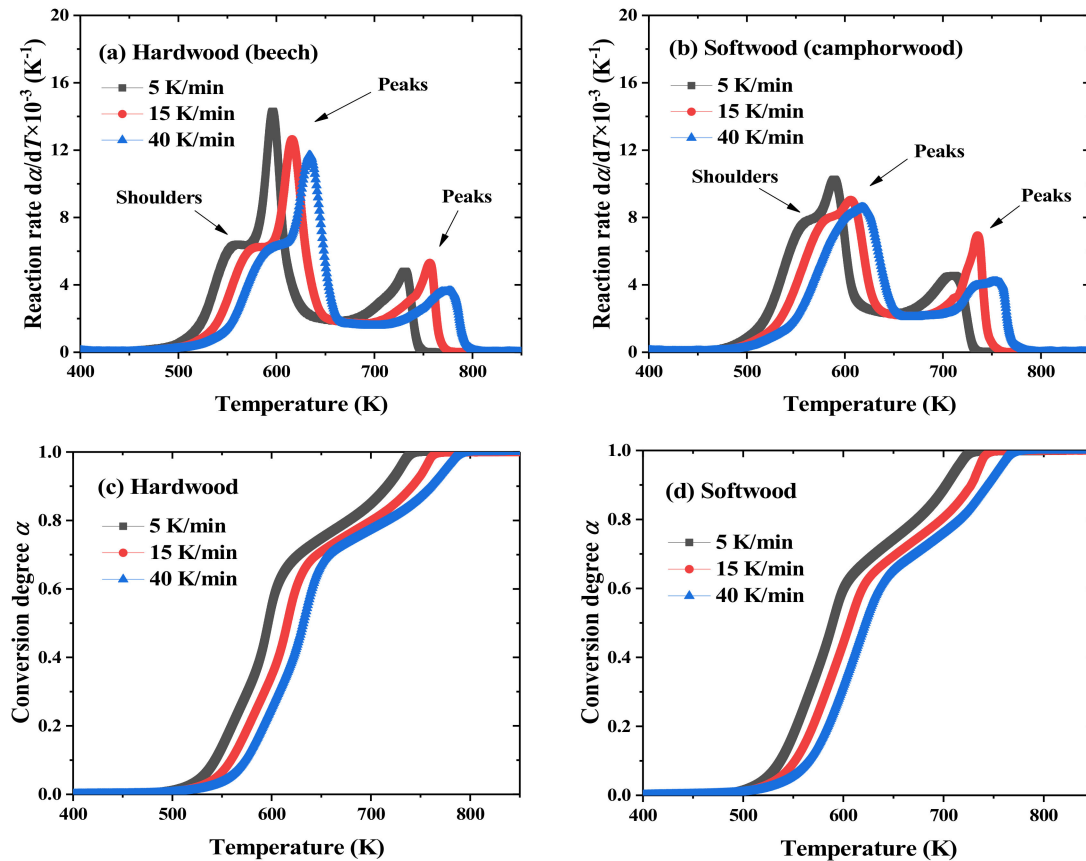


Figure 2. The $d\alpha/dT$ and α curves of beech and camphorwood degradation at various heating rates.

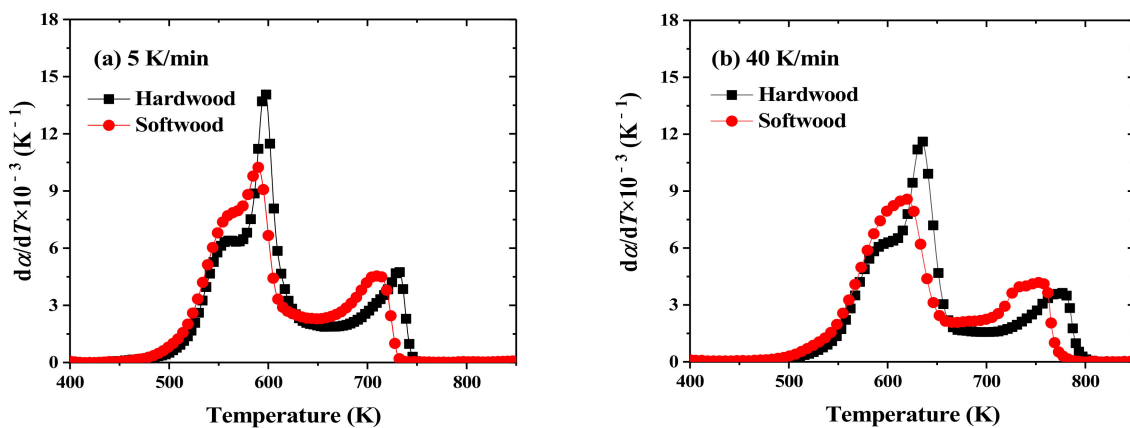


Figure 3. The $d\alpha/dT$ curves of beech and camphorwood under 5 and 40 K/min.

Table 2. The details of hardwood and softwood decomposition based upon α and $d\alpha/dT$.

Sample	Heating Rate (K/min)	Decomposition Temperature Range (K)	Shoulder Temperature (K)/Reaction Rate (K ⁻¹)/Conversion Degree α	First Peak Temperature (K)/Reaction Rate (K ⁻¹)/Conversion Degree α	Second Peak Temperature (K)/Reaction Rate (K ⁻¹)/Conversion Degree α
Hardwood	5	451–753	560.82/6.41 × 10 ⁻³ /0.21	596.27/14.30 × 10 ⁻³ /0.50	730.93/4.80 × 10 ⁻³ /0.96
	15	459–781	582.49/6.25 × 10 ⁻³ /0.23	616.05/12.65 × 10 ⁻³ /0.50	756.53/5.30 × 10 ⁻³ /0.96
	40	469–810	596.61/6.23 × 10 ⁻³ /0.23	634.01/11.69 × 10 ⁻³ /0.52	776.22/3.63 × 10 ⁻³ /0.96
Softwood	5	441–738	564.67/7.88 × 10 ⁻³ /0.29	589.10/10.26 × 10 ⁻³ /0.50	711.54/4.55 × 10 ⁻³ /0.94
	15	444–765	585.76/8.03 × 10 ⁻³ /0.32	606.09/9.04 × 10 ⁻³ /0.49	735.42/6.93 × 10 ⁻³ /0.95
	40	448–795	606.66/8.25 × 10 ⁻³ /0.37	618.12/8.59 × 10 ⁻³ /0.47	752.70/4.18 × 10 ⁻³ /0.94

3.2. Kinetic and Thermodynamic Analysis

3.2.1. Activation Energy by KAS Approach

Activation energy represents the minimum energy required to initiate a reaction. The activation energy has little change with the conversion degree in one certain thermal degradation stage, indicating that the degradation stage is controlled by a one-step reaction [45]. In addition, the activation energy has a significant effect on the reaction rate.

Based upon the KAS approach, with the conversion degree, α , chosen from 0.1 to 0.9, the plots of $\ln(\beta/T^2)$ versus $1/T$ are depicted in Figure 4a,b for hardwood and softwood, respectively. Then, the values of activation energy were computed by the slopes ($-E_\alpha/R$) of the linear regression equation at different conversion degrees, as illustrated in Table 3 and Figure 5.

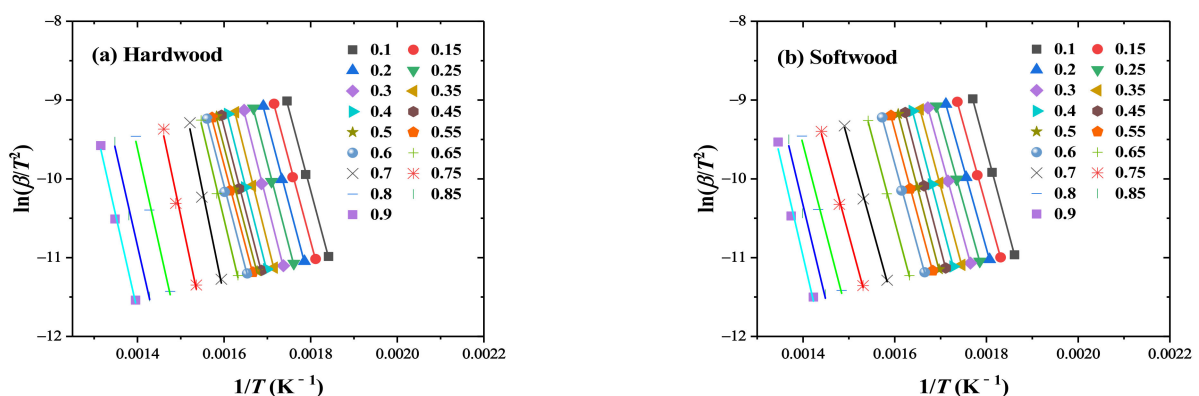
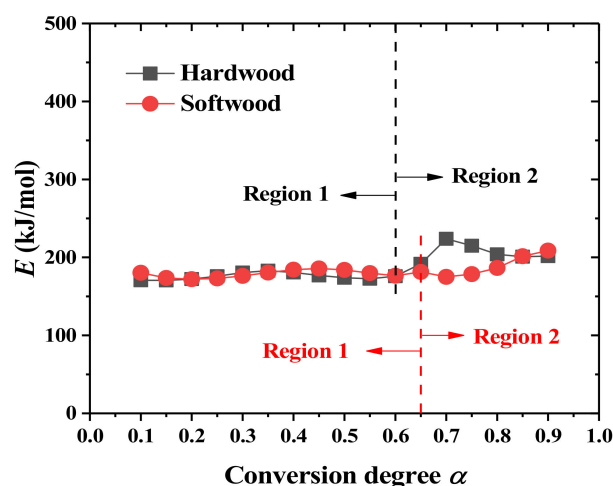
**Figure 4.** The plots of the KAS method at different conversion degrees for (a) hardwood and (b) softwood.**Figure 5.** The activation energy as a function of conversion degree for hardwood and softwood.

Table 3. E , A , and R^2 values for hardwood and softwood based upon the KAS method.

α	Hardwood			Softwood			Standard Deviation of E Values	Standard Deviation of A Values
	E (kJ/mol)	R^2	A (min^{-1})	E (kJ/mol)	R^2	A (min^{-1})		
0.10	170.62	0.9985	29.99	180.31	0.9997	32.72	4.85	1.37
0.15	170.42	0.9984	30.14	173.60	0.9997	31.40	1.59	0.63
0.20	172.22	0.9982	30.60	172.01	0.9998	31.17	0.11	0.29
0.25	175.89	0.9981	31.34	173.03	0.9999	31.46	1.43	0.06
0.30	180.56	0.9975	32.21	176.30	1.0000	32.18	2.13	0.02
0.35	182.94	0.9968	32.57	180.53	1.0000	33.06	1.21	0.25
0.40	180.64	0.9961	32.02	184.21	1.0000	33.80	1.79	0.89
0.45	176.89	0.9964	31.24	185.83	0.9998	34.10	4.47	1.43
0.50	173.87	0.9967	30.66	183.91	0.9993	33.68	5.02	1.51
0.55	172.59	0.9969	30.42	179.80	0.9993	32.82	3.61	1.20
0.60	175.92	0.9962	31.06	176.45	0.9993	32.05	0.27	0.50
0.65	191.68	0.9940	-	181.35	0.9986	32.61	5.17	-
0.70	223.85	0.9753	-	175.02	0.9974	-	24.42	-
0.75	214.93	0.9706	-	178.48	0.9948	-	18.23	-
0.80	203.91	0.9815	-	186.50	0.9875	-	8.71	-
0.85	200.89	0.9858	-	201.42	0.9725	-	0.27	-
0.90	201.56	0.9888	-	208.64	0.9700	-	3.54	-
Average 1	175.69	0.9973	31.11	178.73	0.9997	32.59	1.52	-
Average 2	206.14	0.9827	-	188.57	0.9868	-	8.79	0.74
Average	186.43	0.9921	-	182.20	0.9952	-	2.12	-

For hardwood, the E value remained at about 175 kJ/mol from $\alpha = 0.1$ to $\alpha = 0.6$, and then it varied largely in the range of 0.6–0.9. The process of hardwood degradation can be divided into regions 1 and 2 by the inflection point of 0.6 conversion degree. The average E estimates were 175.69 and 206.14 kJ/mol for regions 1 and 2, respectively. For softwood, the E value remained at about 178 kJ/mol from $\alpha = 0.1$ to $\alpha = 0.65$, and then it rose from 181.35 to 208.64 kJ/mol in the range of 0.65–0.9. Similarly, the process of softwood decomposition can be divided into region 1 ($0 \leq \alpha \leq 0.65$) and region 2 ($0.65 < \alpha \leq 1$). The mean E estimates were 178.73 and 188.57 kJ/mol for regions 1 and 2, respectively. To sum up, the thermal degradation occurring in region 1 for both hardwood and softwood is controlled by a one-step reaction. It is noted that the valuable products were mainly released in the decomposition reaction of region 1. Besides, the mean E value of hardwood was greater than that of softwood in the whole decomposition process. It is indicated that the occurrence of the thermal degradation of softwood was easier than hardwood.

3.2.2. Kinetic Mechanisms by the CR Approach

As demonstrated in Section 3.2.1, the average E values in region 1 estimated by the KAS method were 175.69 and 178.73 kJ/mol for beech and camphorwood, respectively. However, the kinetic model $g(\alpha)$ and A values in region 1 have not been revealed. The CR approach was employed to determine $g(\alpha)$ and A values in this section. The above three kinetic parameters will be used for kinetic modeling in the next section.

The activation energy, pre-exponential factor, and corresponding correlation coefficient, R^2 , values of region 1 estimated via the CR approach with multiple kinetic models for hardwood and softwood are demonstrated in Tables 4 and 5, respectively. If the average E value of region 1 estimated using the CR approach with a given kinetic model is near the mean E value acquired via the KAS approach, the decomposition reaction occurring in region 1 is controlled by the given kinetic model.

Table 4. E , $\ln A$, and R^2 values of hardwood computed via the CR approach with 18 kinetic models at different heating rates in region 1.

No.	$g(\alpha)$	5 K/min			15 K/min			40 K/min			Average Value		
		E (kJ/mol)	$\ln A$ (min ⁻¹)	R^2	E (kJ/mol)	$\ln A$ (min ⁻¹)	R^2	E (kJ/mol)	$\ln A$ (min ⁻¹)	R^2	E (kJ/mol)	$\ln A$ (min ⁻¹)	R^2
1	$\alpha^{3/2}$	111.54	19.78	0.9722	115.1	21.19	0.9769	116.54	21.56	0.9772	114.39	20.84	0.9754
2	$\alpha^{1/2}$	30.86	2.92	0.9586	31.88	4.3	0.9656	32.2	4.86	0.9658	31.65	4.03	0.9633
3	$\alpha^{1/3}$	17.41	-0.25	0.9415	18.01	1.13	0.9512	18.15	1.72	0.9512	17.86	0.87	0.948
4	$\alpha^{1/4}$	10.69	-2.03	0.9127	11.08	-0.65	0.927	11.12	-0.05	0.9262	10.96	-0.91	0.922
5	$-\ln(1-\alpha)$	85.95	15.04	0.9884	87.18	16.1	0.9898	88.27	16.54	0.9907	87.13	15.89	0.9896
6	$(1-\alpha)^{-1}-1$	103.3	19.09	0.9936	102.98	19.7	0.9941	104.31	20.12	0.9956	103.53	19.64	0.9944
7	$(1-\alpha)^{-2}-1$	123.13	24.38	0.9887	120.82	24.43	0.9903	122.43	24.81	0.9923	122.13	24.54	0.9904
8	$[-\ln(1-\alpha)]^{2/3}$	54.14	8.28	0.9869	54.88	9.44	0.9883	55.52	9.95	0.9893	54.85	9.22	0.9882
9	$[-\ln(1-\alpha)]^{1/2}$	38.24	4.79	0.985	38.73	5.99	0.9866	39.15	6.54	0.9877	38.71	5.77	0.9864
10	$[-\ln(1-\alpha)]^{1/3}$	22.33	1.1	0.9799	22.58	2.35	0.982	22.78	2.94	0.9833	22.56	2.13	0.9817
11	$[-\ln(1-\alpha)]^{1/4}$	14.38	-0.91	0.972	14.5	0.36	0.9748	14.59	0.96	0.9763	14.49	0.14	0.9744
12	$[-\ln(1-\alpha)]^2$	170.83	32.45	0.9943	172.14	32.98	0.9953	175.97	33.55	0.9961	172.98	32.99	0.9952
13	$[-\ln(1-\alpha)]^3$	276.82	53.96	0.9902	280.99	54.45	0.9913	284.74	54.46	0.9921	280.85	54.29	0.9912
14	$[-\ln(1-\alpha)]^4$	372.26	73.14	0.9904	377.89	73.33	0.9915	382.98	73.13	0.9923	377.71	73.2	0.9914
15	$1-(1-\alpha)^{1/2}$	78.25	12.53	0.9808	80.07	13.77	0.9837	81.05	14.22	0.9843	79.79	13.51	0.9829
16	$1-(1-\alpha)^{1/3}$	80.75	12.71	0.9838	82.38	13.9	0.986	83.4	14.35	0.9867	82.18	13.65	0.9855
17	α^2	151.88	27.88	0.9735	156.7	29.29	0.978	158.71	29.58	0.9783	155.76	28.92	0.9766
18	$\alpha + (1-\alpha)\ln(1-\alpha)$	160.89	29.26	0.9801	165.16	30.5	0.9832	167.29	30.77	0.9837	164.45	30.18	0.9823
19	$1-2/3\alpha-(1-\alpha)^{2/3}$	164.24	28.53	0.9822	168.26	29.7	0.9849	170.44	29.95	0.9854	167.65	29.39	0.9842
20	$[(1-\alpha)^{-1/3}-1]^2$	192.38	34.98	0.9925	194.15	35.48	0.9932	196.72	35.69	0.9942	194.42	35.38	0.9933

Table 5. E , $\ln A$, and R^2 values of softwood computed via the CR approach with 18 kinetic models at different heating rates in region 1.

No.	$g(\alpha)$	5 K/min			15 K/min			40 K/min			Average value		
		E (kJ/mol)	$\ln A$ (min ⁻¹)	R^2	E (kJ/mol)	$\ln A$ (min ⁻¹)	R^2	E (kJ/mol)	$\ln A$ (min ⁻¹)	R^2	E (kJ/mol)	$\ln A$ (min ⁻¹)	R^2
1	$\alpha^{3/2}$	105.58	18.77	0.9478	104.48	18.95	0.9514	104.42	19.35	0.9589	104.83	19.02	0.9527
2	$\alpha^{1/2}$	28.92	2.55	0.9218	28.38	3.29	0.9256	28.21	4.04	0.9357	28.5	3.29	0.9277
3	$\alpha^{1/3}$	16.15	-0.52	0.8892	15.7	0.3	0.8922	15.51	1.11	0.905	15.79	0.3	0.8955
4	$\alpha^{1/4}$	9.76	-2.27	0.8345	9.35	-1.41	0.8343	9.15	-0.59	0.8499	9.42	-1.42	0.8396
5	$-\ln(1-\alpha)$	81.7	14.33	0.9747	80.71	14.67	0.9771	80.5	15.15	0.9818	80.97	14.72	0.9779
6	$(1-\alpha)^{-1}-1$	98.75	18.37	0.9923	97.57	18.58	0.9935	97.24	18.94	0.9952	97.85	18.63	0.9937
7	$(1-\alpha)^{-2}-1$	118.3	23.65	0.998	116.91	23.69	0.9982	116.43	23.94	0.9973	117.21	23.76	0.9978
8	$[-\ln(1-\alpha)]^{2/3}$	51.33	7.8	0.9711	50.58	8.37	0.9737	50.37	8.99	0.9789	50.76	8.39	0.9746
9	$[-\ln(1-\alpha)]^{1/2}$	36.15	4.41	0.9668	35.52	5.09	0.9695	35.3	5.8	0.9754	35.66	5.1	0.9706
10	$[-\ln(1-\alpha)]^{1/3}$	20.96	0.83	0.9551	20.46	1.62	0.958	20.23	2.39	0.9655	20.55	1.61	0.9595
11	$[-\ln(1-\alpha)]^{1/4}$	13.37	-1.14	0.937	12.93	-0.3	0.9396	12.7	0.51	0.9494	13	-0.31	0.942
12	$[-\ln(1-\alpha)]^2$	160.56	30.68	0.9801	160.72	30.8	0.9781	162.88	31.35	0.9796	161.39	30.95	0.9793
13	$[-\ln(1-\alpha)]^3$	263.91	51.91	0.9786	261.48	50.88	0.9808	261.3	50.46	0.9849	262.23	51.09	0.9814
14	$[-\ln(1-\alpha)]^4$	355.02	70.41	0.979	351.86	68.7	0.9812	351.7	67.82	0.9852	352.86	68.98	0.9818
15	$1-(1-\alpha)^{1/2}$	74.15	11.83	0.9605	73.25	12.24	0.9636	73.09	12.76	0.9699	73.5	12.28	0.9647
16	$1-(1-\alpha)^{1/3}$	76.59	12.01	0.9657	75.67	12.4	0.9685	75.49	12.91	0.9743	75.92	12.44	0.9695
17	α^2	143.91	26.55	0.9502	142.53	26.45	0.9538	142.53	26.66	0.9609	142.99	26.55	0.955
18	$\alpha + (1-\alpha)\ln(1-\alpha)$	152.72	27.91	0.9602	151.23	27.74	0.9634	151.17	27.9	0.9696	151.71	27.85	0.9644
19	$1-2/3\alpha-(1-\alpha)^{2/3}$	156	27.18	0.9637	154.48	26.97	0.9667	154.4	27.11	0.9726	154.96	27.09	0.9677
20	$[(1-\alpha)^{-1/3}-1]^2$	183.6	33.59	0.9841	181.77	33.16	0.986	181.5	33.12	0.9893	182.29	33.29	0.9865

For hardwood, there is a big difference between the average E value attained by the CR approach with the power law, reaction order, contracting, and diffusion models, and that acquired by the KAS method in region 1. However, for the Avrami-Erofeev model, $g(\alpha) = [-\ln(1-\alpha)]^2$, the mean E value (172.98 kJ/mol) is closest to the value (175.69 kJ/mol) calculated via the KAS approach, and the corresponding correlation coefficient, R^2 , is much higher. Thus, the Avrami-Erofeev model, $g(\alpha) = [-\ln(1-\alpha)]^2$, is in charge of the thermal decomposition of hardwood in region 1. For softwood, the mean E value (178.73 kJ/mol) estimated using the 3D diffusional model, $g(\alpha) = [(1-\alpha)^{-1/3}-1]^2$, is near the calculated value (182.29 kJ/mol) of the KAS approach. The corresponding correlation coefficient, R^2 , exceeds 0.98. The most closely matched model for characterizing the degradation process of softwood in region 1 is the 3D diffusion model. Moreover, the pre-exponential factor A of hardwood and softwood in region 1 is obtained based upon the acquired kinetic models, as shown in Table 3. The pre-exponential factor represents the collision frequency between molecules in a reactive system, and the A value higher than 10^9 s^{-1} ($\ln A = 24.82 \text{ min}^{-1}$)

means that the reactive system has high reactivity. The A values of hardwood and softwood in region 1 are all greater than 24.82 min^{-1} . The average $\ln A$ value of hardwood is smaller than that of softwood in region 1.

As shown in Equation (11), the kinetic compensation effect (KCE) [46] is a linear relationship between E and $\ln A$ at various heating rates. E and $\ln A$ show a strong linear relationship, suggesting that the E and $\ln A$ estimates computed using the CR approach with 18 kinetic models are reasonable and convincing.

$$\ln A = a + bE \quad (11)$$

where a is a constant expressed as $a = \ln(k_{iso})$. b is also a constant expressed as $b = 1/(RT_{iso})$. k_{iso} denotes the isokinetic rate constant and T_{iso} represents the isokinetic temperature.

Figure 6a,b illustrate the kinetic compensation effect for hardwood and softwood in region 1 at multiple heating rates, respectively. The detailed information about “KCE” parameters is listed in Table 6. If the T_{iso} value is covered by the temperature range of region 1, then a strong linear relationship between E and $\ln A$ will occur in region 1 [45]. As shown in Table 6, the T_{iso} values are among the temperature range of region 1 under three heating rates for both hardwood and softwood. All the corresponding R^2 values are much higher. As a consequence, the E and $\ln A$ estimates acquired by the CR approach for hardwood and softwood are reasonable and convincing.

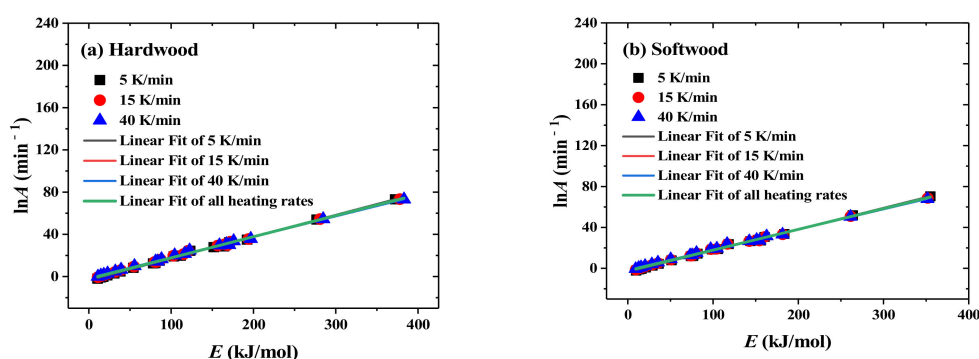


Figure 6. The kinetic compensation effect of region 1 for (a) hardwood and (b) softwood.

Table 6. KCE parameters and corresponding R^2 .

Sample	β (K/min)	a (s^{-1})	95% CI of a	b (mol/kJ)	95% CI of b	k_{iso}	T_{iso} (K)	R^2	Temperature Range of Region 1 (K)
Hardwood	5	-3.3864	(-3.7181, -3.0547)	0.2059	(0.2036, 0.2082)	0.0338	584.16	0.9977	400–605
	15	-2.0282	(-2.3536, -1.7028)	0.1997	(0.1975, 0.2019)	0.1316	602.30	0.9977	400–624
	40	-1.3764	(-1.7022, -1.0506)	0.1948	(0.1926, 0.1970)	0.2525	617.45	0.9976	400–641
	Total heating rates	-2.2630	(-2.4769, -2.0491)	0.2001	(0.1986, 0.2015)	0.1040	601.09	0.9969	-
Softwood	5	-3.4308	(-3.7637, -3.0979)	0.2084	(0.2060, 0.2108)	0.0324	577.15	0.9975	400–613
	15	-2.4137	(-2.7468, -2.0805)	0.2025	(0.2001, 0.2050)	0.0895	593.97	0.9973	400–632
	40	-1.4932	(-1.8264, -1.1599)	0.1975	(0.2000, 0.1951)	0.2247	609.01	0.9971	400–648
	Total heating rates	-2.4441	(-2.6568, -2.2314)	0.2028	(0.2013, 0.2044)	0.0868	593.09	0.9966	-

3.2.3. Thermodynamic Analyses

The values of the changes in enthalpy (ΔH), Gibbs free energy (ΔG), and entropy (ΔS) of hardwood and softwood in region 1 were estimated from the thermogravimetric data at the heating rate of 15 K/min, as listed in Table 7. The difference between E and ΔH

represents the potential energy barrier in the process of biomass combustion [44]. The smaller the potential energy barrier, the easier the reactants transform into products. At the same conversion degree, the difference between E and ΔH of hardwood is greater than that of softwood. This implies that the combustion reaction of softwood occurs easier than that of hardwood. The ΔS values of hardwood and softwood are all positive, implying that their combustion processes raise the disorder degree of the reactive system.

Table 7. H , ΔG , and ΔS values of hardwood and softwood at 15 K/min.

Conversion Degree, α	Hardwood			Softwood		
	ΔH (kJ/mol)	ΔG (kJ/mol)	ΔS (J/(mol·K))	ΔH (kJ/mol)	ΔG (kJ/mol)	ΔS (J/(mol·K))
0.1	165.97	171.63	16.73	175.72	152.63	38.10
0.15	165.69	170.63	16.26	168.93	152.82	26.59
0.2	167.43	170.11	19.17	167.27	152.86	23.78
0.25	171.03	169.96	25.19	168.24	152.83	25.41
0.3	175.63	170.17	32.88	171.45	152.74	30.88
0.35	177.94	170.69	36.74	175.63	152.62	37.96
0.4	175.59	171.23	32.82	179.26	152.52	44.12
0.45	171.81	171.47	26.50	180.84	152.47	46.79
0.5	168.75	171.44	21.39	178.87	152.53	43.46
0.55	167.43	171.36	19.20	174.71	152.64	36.42
0.6	170.73	171.44	24.71	171.30	152.73	30.63
0.65	-	-	-	176.09	152.60	38.77
Average value	170.73	170.92	24.69	174.03	152.67	35.24

ΔG denotes the incremental energy of the reactive system and the direction of the combustion reaction. The ΔG value of hardwood is larger than that of softwood, which shows that the hardwood combustion is more difficult to be carried out than softwood combustion. The ΔG values of hardwood (beech wood) and softwood (camphorwood) are similar to other biomass raw materials, such as waste tea [47], cattle manure [48], and *Lentinus edodes* [49], which proves that beech wood and camphorwood can be appropriate biomass raw materials for bioenergy production.

3.3. Kinetic Modeling

Based upon the estimated kinetic triplet (E , A , and kinetic model), the kinetic modeling for the thermal degradation process of hardwood and softwood in region 1 is conducted in this section. The mathematical expression of the conversion degree, α , for hardwood and softwood can be derived from the obtained kinetic model combined with Equation (5), as presented in Equations (12) and (13):

$$\alpha = 1 - \text{EXP} \left[- \left(\frac{v(y-2)e^{-y}}{y^3} \right)^{\frac{1}{2}} \right] \quad (12)$$

$$\alpha = 1 - \left[1 + \left(\frac{v(y-2)e^{-y}}{y^3} \right)^{\frac{1}{2}} \right]^{-3} \quad (13)$$

where $v = AE/\beta R$ and $y = E/RT$.

Figure 7a,b show the experimental and simulated conversion degree curves under 5, 15, 20, and 40 K/min for beech and camphorwood, respectively. The simulated result is extremely consistent with the experimental results for hardwood and softwood at four different heating rates, and the correlation coefficients are greater than or equal to 0.9988 for both hardwood and softwood. Consequently, the estimated kinetic triplet can perfectly simulate the thermal degradation process of hardwood and softwood in region 1 at 5, 15, 20, and 40 K/min. It is noted that the kinetic triplet used for modeling the thermal

degradation process was obtained on the basis of the thermogravimetric experimental profile at 5, 15, and 40 K/min. However, the experimental profile under 20 K/min was not used for calculating the kinetic triplet.

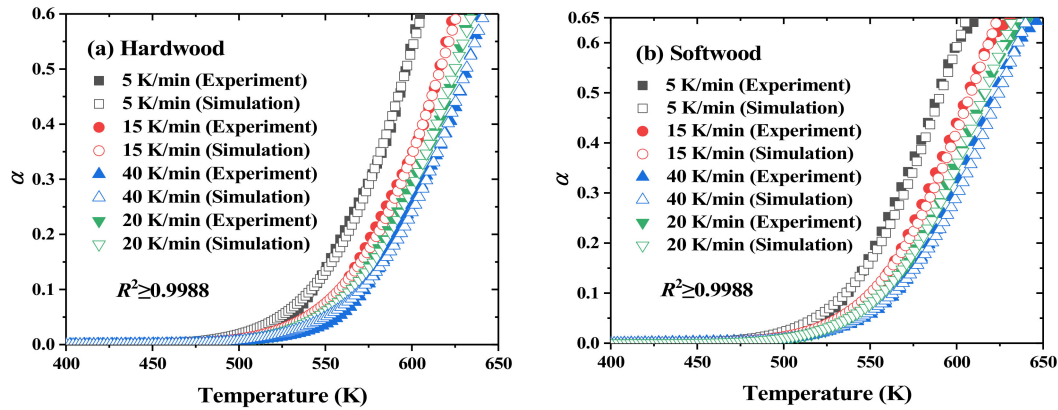


Figure 7. Comparison of the experiment with simulation at multiple heating rates.

3.4. Combustion Characteristic Parameters' Analysis

Based upon the method illustrated in Section 2.4, the characteristic temperature of hardwood and softwood combustion is obtained from TG and DTG curves, as presented in Table 8. As illustrated in Table 8, the T_i , T_p , and T_b values of hardwood and softwood exhibit an increasing trend with the increased heating rate, which means that heating rate has a delayed effect on biomass combustion. This can be explained by the thermal hysteresis effect. At the same heating rate, the ignition temperature, T_i , of softwood is lower than that of hardwood, indicating that softwood is easier to ignite than hardwood. In addition, compared with softwood, the maximum combustion rate, $-R_p$, of hardwood is higher, which implies that the burning reaction of hardwood is more intense.

Table 8. Combustion characteristic parameters of hardwood and softwood.

Biomass	$\beta/\text{K min}^{-1}$	Temperature/K			$-R_p/\%$ min^{-1}	Time/min			Combustion Parameters	
		T_i	T_p	T_b		t_i	t_p	t_b	$C/10^{-4}\%$ $\text{min}^{-1} \text{K}^{-2}$	$C_b/10^{-4}$ min^{-1}
Hardwood	5	561.19	596.44	748.24	6.60	47.61	54.66	85.02	0.21	18.19
	15	578.20	616.05	770.28	17.51	17.00	19.56	29.81	0.52	52.22
	40	589.01	634.01	800.23	42.13	6.65	7.77	11.93	1.21	117.80
Softwood	5	541.56	590.13	733.28	4.79	43.68	53.40	82.03	0.16	12.22
	15	553.18	606.63	758.98	12.38	15.34	18.90	29.06	0.40	30.07
	40	563.29	616.58	787.57	32.17	6.00	7.34	11.61	1.01	70.23

To compare the combustion performance of hardwood and softwood, two combustion characteristic indexes are described, as [50]:

$$C = (-R_p)/T_i^2 \quad (14)$$

$$C_b = \frac{(f_1 \times f_2)}{t_b} \quad (15)$$

where f_1 and f_2 correspond to the mass loss fraction before and after the ignition point. f_1 reflects the content ratio of volatiles, which relates with the effect of the ignition characteristic of biomass, while f_2 reflects the burnout character of biomass, which relates with the carbon contents and configuration of biomass. C represents the reactivity of biomass at the ignition point, and C_b describes the burnout characteristics and stability of biomass. The greater their value, the higher the combustion performance is.

As illustrated in Table 8, with the increase of heating rate, the C and C_b values of hardwood and softwood apparently increase, which indicates that the heating rate has a significant promoting effect on combustion performance. The larger C value of one certain biomass means that it has better thermal degradation stability after ignition. It is worth noting that the C value of hardwood is higher than that of softwood at the same heating rate, implying that the thermal degradation stability of hardwood is higher than that of softwood. Moreover, the C_b value of hardwood is higher than that of softwood at each heating rate, indicating that hardwood has better burnout characteristics. In conclusion, the combustion performance of hardwood is superior to softwood under the same external conditions (heating rate and atmosphere).

4. Conclusions

The main aim of this study was to provide guidance for utilizing woody biomass effectively for bioenergy and chemical feedstocks during the thermal degradation process. The thermal degradation characteristics and kinetic mechanisms of typical hardwood (beech wood) and softwood (camphorwood) were studied by employing a thermogravimetric analyzer at the heating rates of 5, 15, 20, and 40 K/min under air. The KAS approach combined with the CR approach was applied to estimate the kinetic triplet.

- (1) Softwood decomposition began and ended at lower temperatures than hardwood in air atmosphere. Two diverse peaks and one shoulder appeared on the reaction rate curves for both hardwood and softwood. The maximal reaction rate of hardwood was larger than that of softwood.
- (2) The activation energy was maintained at a constant in the conversion degree range of 0.1–0.6 for hardwood, while 0.1–0.65 for softwood. The thermal degradation process can be divided into two regions by the dividing points of $\alpha = 0.6$ and $\alpha = 0.65$ for hardwood and softwood, respectively. The mean E value of hardwood was larger than that of softwood during the whole decomposition process.
- (3) The thermal degradation process occurring in region 1 was dominated by the Avrami-Erofeev model ($g(\alpha) = [-\ln(1 - \alpha)]^2$) and the 3D diffusional model ($g(\alpha) = [(1 - \alpha)^{-1/3} - 1]^2$) for hardwood and softwood, respectively. The average A value of softwood was larger than that of hardwood in region 1.
- (4) The simulated conversion degree curves were consistent with the experimental curves at 5, 15, 20, and 40 K/min. Therein, the thermogravimetric experimental profile under 20 K/min was not used for estimating the kinetic triplet.
- (5) The values of ignition temperature (T_i), peak temperature (T_{max}), and burnout temperature (T_b) for both hardwood and softwood exhibited an increasing trend with the increased heating rate. Under the same external conditions (heating rate and atmosphere), the combustion performance of hardwood was superior to softwood.

Author Contributions: Conceptualization, X.X. and R.C.; investigation and experiment, X.X. and R.C.; writing—original draft X.X. and R.P.; writing-review and editing, X.X., R.C. and R.P. All authors have read and agreed to the published version of the manuscript.

Funding: This work was supported by the National Natural Science Foundation of China (No. 51806106), and the Science and Technology Department of Jiangsu Province, China (No: BK20170838).

Institutional Review Board Statement: Not applicable.

Informed Consent Statement: Not applicable.

Data Availability Statement: The data will be made available on request from the corresponding author.

Conflicts of Interest: The authors declare no conflict of interest.

References

1. Zhang, W.; Zhang, J.; Ding, Y.; He, Q.; Lu, K.; Chen, H. Pyrolysis kinetics and reaction mechanism of expandable polystyrene by multiple kinetics methods. *J. Clean. Prod.* **2021**, *285*, 125042. [[CrossRef](#)]
2. Jia, G. Combustion Characteristics and Kinetic Analysis of Biomass Pellet Fuel Using Thermogravimetric Analysis. *Processes* **2021**, *9*, 868. [[CrossRef](#)]
3. Cao, W.; Li, W.; Yu, S.; Zhang, Y.; Shu, C.-M.; Liu, Y.; Luo, J.; Bu, L.; Tan, Y. Explosion venting hazards of temperature effects and pressure characteristics for premixed hydrogen-air mixtures in a spherical container. *Fuel* **2021**, *290*, 120034. [[CrossRef](#)]
4. Liu, W.; Yu, Z.; Zhu, Q.; Zhou, X.; Peng, C. Assessment of biomass utilization potential of *Caragana korshinskii* and its effect on carbon sequestration on the Northern Shaanxi Loess Plateau, China. *Land Degrad. Dev.* **2020**, *31*, 53–64. [[CrossRef](#)]
5. Mitchell, J. The “Greenhouse” effect and climate change. *Rev. Geophys.* **1989**, *27*, 115–139. [[CrossRef](#)]
6. Altantzis, A.-I.; Kallistridis, N.-C.; Stavropoulos, G.; Zabaniotou, A. Apparent Pyrolysis Kinetics and Index-Based Assessment of Pretreated Peach Seeds. *Processes* **2021**, *9*, 905. [[CrossRef](#)]
7. Wang, Z.; Wang, J.; Xie, L.; Zhu, H.; Shu, X. Influence of the Addition of Cotton Stalk during Co-pyrolysis with Sewage Sludge on the Properties, Surface Characteristics, and Ecological Risks of Biochars. *J. Therm. Sci.* **2019**, *28*, 755–762. [[CrossRef](#)]
8. López-Beceiro, J.; Díaz-Díaz, A.M.; Alvarez-García, A.; Tarrío-Saavedra, J.; Artiaga, R. The complexity of lignin thermal degradation in the isothermal context. *Processes* **2021**, *9*, 1154. [[CrossRef](#)]
9. Hu, J.; Song, Y.; Liu, J.; Evrendilek, F.; Buyukada, M.; Yan, Y.; Li, L. Combustions of torrefaction-pretreated bamboo forest residues: Physicochemical properties, evolved gases, and kinetic mechanisms. *Bioresour. Technol.* **2020**, *304*, 122960. [[CrossRef](#)]
10. Anca-Couce, A.; Obernberger, I. Application of a detailed biomass pyrolysis kinetic scheme to hardwood and softwood torrefaction. *Fuel* **2016**, *167*, 158–167. [[CrossRef](#)]
11. Magalhães, S.; Filipe, A.; Melro, E.; Fernandes, C.; Vitorino, C.; Alves, L.; Romano, A.; Rasteiro, M.; Medronho, B. Lignin Extraction from Waste Pine Sawdust Using a Biomass Derived Binary Solvent System. *Polymers* **2021**, *13*, 1090. [[CrossRef](#)]
12. Amaral, S.S.; de Carvalho, J.A., Jr.; Costa, M.A.M.; Neto, T.G.S.; Dellani, R.; Leite, L.H.S. Comparative study for hardwood and softwood forest biomass: Chemical characterization, combustion phases and gas and particulate matter emissions. *Bioresour. Technol.* **2014**, *164*, 55–63. [[CrossRef](#)] [[PubMed](#)]
13. Mian, I.; Li, X.; Dacres, O.D.; Wang, J.; Wei, B.; Jian, Y.; Zhong, M.; Liu, J.; Ma, F.; Rahman, N. Combustion kinetics and mechanism of biomass pellet. *Energy* **2020**, *205*, 117909. [[CrossRef](#)]
14. Kosowska-Golachowska, M.; Technology CUo Machinery, I.O.T. Thermal analysis and kinetics of coal during oxy-fuel combustion. *J. Thermal Sci.* **2017**, *26*, 355–361. [[CrossRef](#)]
15. Chen, R.; Li, Q.; Xu, X.; Zhang, D. Comparative pyrolysis characteristics of representative commercial thermosetting plastic waste in inert and oxygenous atmosphere. *Fuel* **2019**, *246*, 212–221. [[CrossRef](#)]
16. Toscano, G.; Duca, D.; Rossini, G.; Mengarelli, C.; Pizzi, A. Identification of different woody biomass for energy purpose by means of Soft Independent Modeling of Class Analogy applied to thermogravimetric analysis. *Energy* **2015**, *83*, 351–357. [[CrossRef](#)]
17. An, W.; Tang, Y.; Liang, K.; Cai, M.; Wang, T.; Wang, Z. Experimental study on downward flame spread characteristics under the influence of parallel curtain wall. *Fractals* **2019**, *62*, 102407. [[CrossRef](#)]
18. Weiguang, A.; Xiangwei, Y.; Minglun, C.; Yunji, G.; Hetang, W. Influence of vertical channel on downward flame spread over extruded polystyrene foam. *Int. J. Thermal Sci.* **2019**, *145*, 105991.
19. An, W.; Tang, Y.; Liang, K.; Cai, M.; Wang, T.; Wang, Z. Study on temperature distribution and CO diffusion induced by cable fire in L-shaped utility tunnel. *Sustain. Cities Soc.* **2020**, *62*, 102407. [[CrossRef](#)]
20. Ding, Y.; Huang, B.; Li, K.; Du, W.; Lu, K.; Zhang, Y. Thermal interaction analysis of isolated hemicellulose and cellulose by kinetic parameters during biomass pyrolysis. *Energy* **2020**, *195*, 117010. [[CrossRef](#)]
21. Polesek-Karczewska, S.; Kardaś, D. Prediction of thermal behavior of pyrolyzed wet biomass by means of model with inner wood structure. *J. Therm. Sci.* **2015**, *24*, 82–89. [[CrossRef](#)]
22. Ding, Y.; Fukumoto, K.; Ezekoye, O.; Lu, S.; Wang, C.; Li, C. Experimental and numerical simulation of multi-component combustion of typical charring material. *Combust. Flame* **2020**, *211*, 417–429. [[CrossRef](#)]
23. Yang, H.; Yan, R.; Chen, H.; Lee, D.H.; Zheng, C. Characteristics of hemicellulose, cellulose and lignin pyrolysis. *Fuel* **2007**, *86*, 1781–1788. [[CrossRef](#)]
24. Slopiecka, K.; Bartocci, P.; Fantozzi, F. Thermogravimetric analysis and kinetic study of poplar wood pyrolysis. *Appl. Energy* **2012**, *97*, 491–497. [[CrossRef](#)]
25. Dong, C.-Q.; Zhang, Z.-F.; Lu, Q.; Yang, Y.-P. Characteristics and mechanism study of analytical fast pyrolysis of poplar wood. *Energy Convers. Manag.* **2012**, *57*, 49–59. [[CrossRef](#)]
26. Zou, H.; Zhang, J.; Liu, J.; Buyukada, M.; Evrendilek, F.; Liang, G. Pyrolytic behaviors, kinetics, decomposition mechanisms, product distributions and joint optimization of *Lentinus edodes* stipe. *Energy Convers. Manag.* **2020**, *213*, 112858. [[CrossRef](#)]
27. Ding, Y.; Ezekoye, O.; Lu, S.; Wang, C.; Zhou, R. Comparative pyrolysis behaviors and reaction mechanisms of hardwood and softwood. *Energy Convers. Manag.* **2017**, *132*, 102–109. [[CrossRef](#)]
28. Yao, F.; Wu, Q.; Lei, Y.; Guo, W.; Xu, Y. Thermal decomposition kinetics of natural fibers: Activation energy with dynamic thermogravimetric analysis. *Polym. Degrad. Stab.* **2008**, *93*, 90–98. [[CrossRef](#)]
29. Echresh Zadeh, Z.; Abdulkhani, A.; Saha, B. Characterization of Fast Pyrolysis Bio-Oil from Hardwood and Softwood Lignin. *Energies* **2020**, *13*, 887. [[CrossRef](#)]

30. Asmadi, M.; Kawamoto, H.; Saka, S. Characteristics of softwood and hardwood pyrolysis in an ampoule reactor. *J. Anal. Appl. Pyrolysis* **2017**, *124*, 523–535. [[CrossRef](#)]
31. Grønli, M.G.; Varhegyi, G.; Di Blasi, C. Thermogravimetric Analysis and Devolatilization Kinetics of Wood. *Ind. Eng. Chem. Res.* **2002**, *41*, 4201–4208. [[CrossRef](#)]
32. Gil, M.; Casal, D.; Pevida, C.; Pis, J.; Rubiera, F. Thermal behaviour and kinetics of coal/biomass blends during co-combustion. *Bioresour. Technol.* **2010**, *101*, 5601–5608. [[CrossRef](#)]
33. Kong, B.; Wang, E.; Li, Z.; Lu, W. Study on the feature of electromagnetic radiation under coal oxidation and temperature rise based on multi-fractal theory. *Fractals* **2019**, *27*, 1950038. [[CrossRef](#)]
34. Cai, P.; Nie, W.; Chen, D.; Yang, S.; Liu, Z. Effect of air flowrate on pollutant dispersion pattern of coal dust particles at fully mechanized mining face based on numerical simulation. *Fuel* **2019**, *239*, 623–635. [[CrossRef](#)]
35. Kissinger, H.E. Variation of peak temperature with heating rate in differential thermal analysis. *J. Res. Natl. Inst. Stand. Technol.* **1956**, *57*, 217. [[CrossRef](#)]
36. Akahira, T.; Sunose, T. Method of determining activation deterioration constant of electrical insulating materials. *Sci. Technol.* **1971**, *16*, 22–31.
37. Coats, A.W.; Redfern, J.P. Kinetic parameters from thermogravimetric data. *Nature* **1964**, *201*, 68–69. [[CrossRef](#)]
38. Xu, X.; Pan, R.; Li, P.; Chen, R. Kinetics, Thermodynamics, and Volatile Products of Camphorwood Pyrolysis in Inert Atmosphere. *Appl. Biochem. Biotechnol.* **2020**, 1–19. [[CrossRef](#)]
39. Qiao, Y.; Das, O.; Zhao, S.-N.; Sun, T.-S.; Xu, Q.; Jiang, L. Pyrolysis Kinetic Study and Reaction Mechanism of Epoxy Glass Fiber Reinforced Plastic by Thermogravimetric Analyzer (TG) and TG-FTIR (Fourier-Transform Infrared) Techniques. *Polymers* **2020**, *12*, 2739. [[CrossRef](#)]
40. Jiang, H.; Wang, J.; Wu, S.; Wang, B.; Wang, Z. Pyrolysis kinetics of phenol-formaldehyde resin by non-isothermal thermogravimetry. *Carbon* **2010**, *48*, 352–358. [[CrossRef](#)]
41. Vlaev, L.; Nedelchev, N.; Gyurova, K.; Zagorcheva, M. A comparative study of non-isothermal kinetics of decomposition of calcium oxalate monohydrate. *J. Anal. Appl. Pyrolysis* **2008**, *81*, 253–262. [[CrossRef](#)]
42. Liqing, L.; Donghua, C. Application of iso-temperature method of multiple rate to kinetic analysis. *J. Therm. Anal. Calorim.* **2004**, *78*, 283–293. [[CrossRef](#)]
43. Chen, R.; Li, Q.; Zhang, Y.; Xu, X.; Zhang, D. Pyrolysis kinetics and mechanism of typical industrial non-tyre rubber wastes by peak-differentiating analysis and multi kinetics methods. *Fuel* **2019**, *235*, 1224–1237. [[CrossRef](#)]
44. Wu, X.; Wei, Z.; Liu, J.; Chen, Z.; Huang, W. Oxy-fuel and air combustion performances and gas-to-ash products of aboveground and below ground biomass of *Sedum alfredii* Hance. *Chem. Eng. J.* **2021**, *422*, 130312. [[CrossRef](#)]
45. Jiang, L.; Zhang, D.; Li, M.; He, J.-J.; Gao, Z.-H.; Zhou, Y.; Sun, J.-H. Pyrolytic behavior of waste extruded polystyrene and rigid polyurethane by multi kinetics methods and Py-GC/MS. *Fuel* **2018**, *222*, 11–20. [[CrossRef](#)]
46. Vyazovkin, S.; Burnham, A.; Criado, J.M.; Perez-Maqueda, L.A.; Popescu, C.; Sbirrazzuoli, N. ICTAC Kinetics Committee recommendations for performing kinetic computations on thermal analysis data. *Thermochim. Acta* **2011**, *520*, 1–19. [[CrossRef](#)]
47. Cai, H.; Zou, H.; Liu, J.; Xie, W.; Kuo, J.; Buyukada, M.; Evrendilek, F. Thermal degradations and processes of waste tea and tea leaves via TG-FTIR: Combustion performances, kinetics, thermodynamics, products and optimization. *Bioresour. Technol.* **2018**, *268*, 715–725. [[CrossRef](#)] [[PubMed](#)]
48. Zhang, J.; Liu, J.; Evrendilek, F.; Xie, W.; Kuo, J.; Zhang, X.; Buyukada, M. Kinetics, thermodynamics, gas evolution and empirical optimization of cattle manure combustion in air and oxy-fuel atmospheres. *Appl. Therm. Eng.* **2019**, *149*, 119–131. [[CrossRef](#)]
49. Zou, H.; Evrendilek, F.; Liu, J.; Buyukada, M. Combustion behaviors of pileus and stipe parts of *Lentinus edodes* using thermogravimetric-mass spectrometry and Fourier transform infrared spectroscopy analyses: Thermal conversion, kinetic, thermodynamic, gas emission and optimization analyses. *Bioresour. Technol.* **2019**, *288*, 121481. [[CrossRef](#)]
50. Li, Q.; Zhao, C.; Chen, X.; Wu, W.; Li, Y. Comparison of pulverized coal combustion in air and in O₂/CO₂ mixtures by thermo-gravimetric analysis. *J. Anal. Appl. Pyrolysis* **2009**, *85*, 521–528. [[CrossRef](#)]